Natural Resources for Human Health
eISSN: 2583-1194

Original Research

Received 02 July 2026
Revised 23 Aug 2026
Accepted 06 Sep 2026

Natural Resources for Human Health 2026, Vol. 6 (19s): 654–670

KEYWORDS:
Artificial Intelligence, Digital Healthcare, Intelligent Health Sensing, Multifunctional Biomaterial, Personalized Healthcare, Wearable Biosensors.

IoT-Enabled Multifunctional Biomaterials for Continuous Health Sensing and Intelligent Digital Healthcare Service Loops

Dongzhu Zhang[1]*

[1]Central South University,932 Lushan South Road, Changsha, Hunan, 410083, China
Email: 13780158190@163.com

ABSTRACT: The continuous monitoring of health using IoT-based multifunctional biomaterials for personalized healthcare is possible, but the existing systems are limited by noise, signal variations, multimodal complexity and unreliable health-risk prediction. To address the limitation, this research proposes an algorithm called Vital Intelligence Temporal Adaptation Learning Integrated Sensing Network (VITALIS-Net), which combines three key approaches, Adaptive Kalman Filter (AKF), Multimodal Temporal Transformer (MTT) and Deep Evidential Learning (DEL). Continuous signals generated by multifunctional wearable sensors based on biomaterial are collected using IoT network. In this context, AKF does adaptive denoising and measurement corrections, while MTT used in extracting temporal dependencies and fusion of multiple modalities from the sensors. Finally, DEL facilitates uncertainty-based health-risk predictions. The developed framework is a digital healthcare service loop of continuous sensing, health risk detection, intelligent feedback and re-monitoring. This research evaluates the performance of the framework with respect to predictive reliability against drifting sensors, missed measurements and changes in physiological states. Health-risk classification accuracy obtained using the proposed VITALIS-Net is 98.2%. Overall the VITALIS-Net can support and efficiently personalized healthcare with dependable adaptive signal denoising, multimodal temporal analysis, health risk predictions with uncertainty and intelligent monitoring.

1. INTRODUCTION

Recent advances in wearable health monitoring and intelligent health-care systems have received considerable attention because of the rising demand for continuous, non-invasive and real-time monitoring of physiology. Multimodal deep learning and wearable sensors for fall risk prediction and real-time alarms for elder care has been researched in recent years [1]. Wearable biosensors integrated with Artificial Intelligence (AI) technologies have also been used for continuous health monitoring [2]. In addition to this, multimodal cardiovascular risk prediction with clinical and wearable sensors has been performed using spatio-temporal transformers [3].The issues of signal quality and accurate processing of physiological data have continued to be an active area of research in the domain of wearable health care solutions. The process of Electrocardiogram (ECG) signal denoising using stationary wavelet transform has been considered as a method to enhance the quality of physiological signals captured by wearable devices [4]. Missing data problems in the context of wearable diabetes monitoring have been researched to analyze the reasons of the data loss and increase the accuracy of health status assessment [5]. Moreover, the use of transformer architecture for classification of affective states via wearable [6] physiological signals has been researched.

Even though all these developments have taken place, most of the previous research has been centered around on individual diseases, certain physiological signals or specific tasks of detection and prediction. The unification of heterogeneous signals

from wearables, effective signal quality management, multimodal feature fusion, personalized prediction and real-time healthcare feedback is an area where further research is needed. Hence, for this reason, this research proposed a wearable healthcare framework known as the Vital Intelligence Temporal Adaptation Learning Integrated Sensing Network (VITALIS-Net). The proposed VITALIS-Net incorporates three core algorithms, namely the Adaptive Kalman Filter (AKF) for adaptive signal denoising and measurement correction, the Multimodal Temporal Transformer (MTT) for temporal dependency extraction and heterogeneous multimodal feature fusion and Deep Evidential Learning (DEL) for uncertainty-aware health-risk prediction.

The main contributions of this research are:

- The IoT-enabled multifunctional biomaterial sensing for continuous acquisition and transmission of physiological and biochemical health signals.
- Adaptive Kalman Filter (AKF) for reducing sensor noise, correcting measurements and improving signal reliability under sensor drift and changing sensing conditions.
- Multimodal Temporal Transformer (MTT) and Deep Evidential Learning (DEL) for temporal multimodal feature integration, uncertainty-aware health-risk prediction and reliable health-state assessment.
- Integrated VITALIS-Net framework for connecting continuous sensing, intelligent health-risk identification, personalized feedback, clinical review support and repeated monitoring within a digital healthcare service loop.

The novelty of VITALIS-Net present in integrating AKF, MTT and DEL within a unified IoT-enabled biomaterial sensing framework for adaptive signal correction, multimodal temporal learning, uncertainty-aware health-risk prediction and personalized healthcare feedback. The proposed scheme offers further assistance in real-time monitoring despite sensor drifts, missing values and variations in the physiological state.

The structure of this research is as follows: Section 2 mentioned previous research regarding the problem, Section 3 presents the proposed approach and its mathematics behind the VITALIS-Net, Section 4 describes about experimental results. Section 5 mentioned the robustness, ablation studies and limitations of the proposed. Finally, Section 6 concludes this research with the future work.

2. LITERATURE REVIEW

V. Suglia et al. (2024) [8] focused on continuous human activity recognition using inertial sensors and deep learning. A Convolutional Neural Network (CNN)-based system recognized seamless activities, but the limited number of participants hindered generalizability, although the accuracy was increased.

U. Debnath and S. Kim (2026) [9] developed Remote Photoplethysmography (rPPG)-based heart-rate monitoring using Discrete Wavelet Transform (DWT), adaptive Kalman filtering, fusion and band-pass filtering. Dataset diversity remained limited, low Mean Absolute Errors (MAEs) demonstrated improved accuracy.

M. Yalcin and M. E. Latoschik (2026) [10] generated Electrocardiogram (ECG) from Photoplethysmography (PPG) using Transformer Generative Adversarial Network (GAN) and self-supervised learning. Motion and signal variability remained challenges, cross-dataset evaluation reduced heart-rate errors substantially.

Z. Wang et al. (2025) [11] developed PhysioFormer using multimodal physiological signals, feature embedding and symbolic regression. Limited data increased overfitting risk, the model achieved over high accuracy and improved explainability

Table 1: Comparative Performance Analysis of the Existing researches

Author, Year [Ref.]	Concept	Method	Limitation	Result
Laudenzi, B. M. et al. (2025) [12]	Wearable signals for disease monitoring	Gaussian Process Regression (GPR) with simulated physiological data	In-silico validation only	Predicted cardiovascular and respiratory

				indicators
Xiang, J.-Z. et al. (2025) [13]	Multimodal stress detection	Convolutional Neural Network (CNN), Fast Fourier Transform (FFT), Synthetic Minority Over-sampling Technique (SMOTE)	Small dataset	Achieved 91% accuracy
Hussain, S. et al. (2025) [14]	Wearable sweat biosensing	Photonic sensor array and microfluidics	Limited human validation	Detected glucose, urea and lactate
Lin, Y. et al. (2025) [15]	Continuous respiratory monitoring	Electrocardiogram (ECG)–Photoplethysmography(PPG) fusion and Principal Component Analysis **(**PCA)	Limited diverse-condition validation	Reduced respiratory-rate estimation error

This table 1 demonstrates the advances in wearable physiological monitoring through machine learning, multimodal signal fusion, photonic biosensing and respiratory analysis. However, limitations remained in real-world validation, dataset diversity, sensor artifacts, clinical generalization and continuous multimodal integration, creating opportunities for more robust intelligent healthcare monitoring frameworks.

2.1 Research Gap

The previous research efforts have shown progress in areas of wearables, multimodal physiology, deep learning and intelligent healthcare prediction. However, there were challenges yet to be resolved such as integrating diverse sensors, coping with missing data, as well as real-time continuous sensing and prediction. Combining biochemical, physiological and behavioral signals along with explainable artificial intelligence were underrepresented as well.

3. PROPOSED METHODOLOGY

This section describes about the VITALIS-Net architecture that is proposed for continuous multi-sensory healthcare monitoring and personalized risk prediction. In the design of the system with architecture, it formulates how wearable sensors, Internet of Things (IoT) data transfer, adaptive Kalman filtering, multimodal temporal transformer and deep evidential learning interact to perform the process.

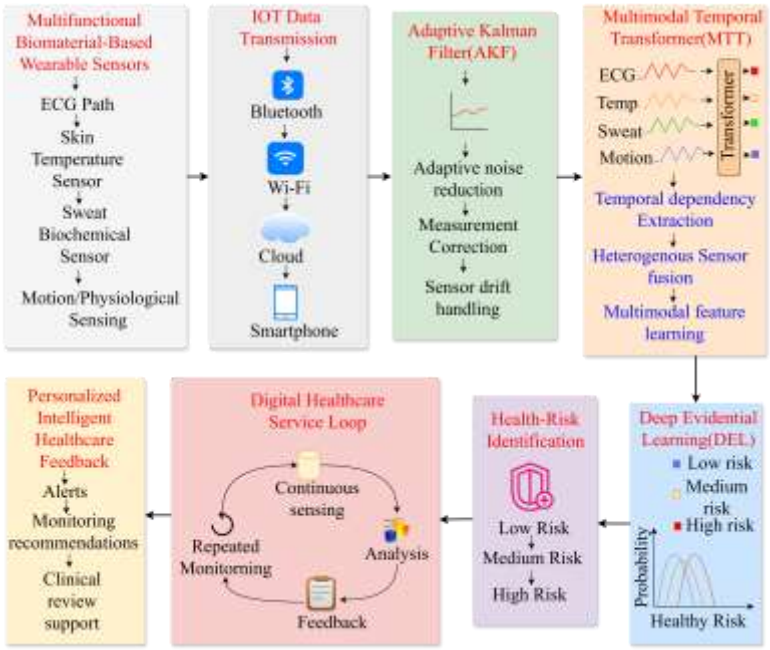


Figure 1: Constantly Intelligent Monitoring of Health State using VITALIS-Net

Natural Resources for Human Health
eISSN: 2583-1194

Figure 1 presents the process flow of the VITALIS-Net, during which wearable multifunctional biomaterial sensors monitor different health parameters and transfer these data through the Internet of Things to be processed through AKF and MTT for signal corrections and temporal multimodal feature fusion correspondingly. This representation is further analyzed through the DEL approach to recognize health risks and provide personalized feedback on health state.

3.2 Continuous Health Sensing and Intelligent Digital Healthcare Service Loops

The proposed Vital Intelligence Temporal Adaptation Learning Integrated Sensing Network (VITALIS-Net) framework utilizes a combination of multifunctional biomaterials, Internet of Things (IoT) communication and artificial intelligence to facilitate continuous monitoring of health conditions via physiological and biochemical health assessment. In the VITALIS-Net algorithm, issues such as sensor noise, variabilities in measurements, multi-modality and uncertainty in predicting the risk of health conditions are considered. VITALIS-Net integrates three core algorithms, Adaptive Kalman Filter (AKF), Multimodal Temporal Transformer (MTT) and Deep Evidential Learning (DEL). AKF performs adaptive signal denoising and measurement correction by adjusting noise estimates according to changing sensor conditions. MTT extracts temporal dependencies and integrates heterogeneous physiological and biochemical features using attention mechanisms. DEL performs uncertainty-aware health-risk classification, distinguishing reliable predictions from uncertain outcomes. Adaptive reproducibility is supported through standardized preprocessing, documented sensor calibration, consistent data partitioning, controlled training configurations and systematic evaluation under changing sensing conditions. Prediction outcomes support personalized feedback, clinical review and repeated monitoring through an intelligent digital healthcare service loop. Consequently, VITALIS-Net establishes an adaptive, reproducible framework for reliable continuous health assessment and personalized digital healthcare.

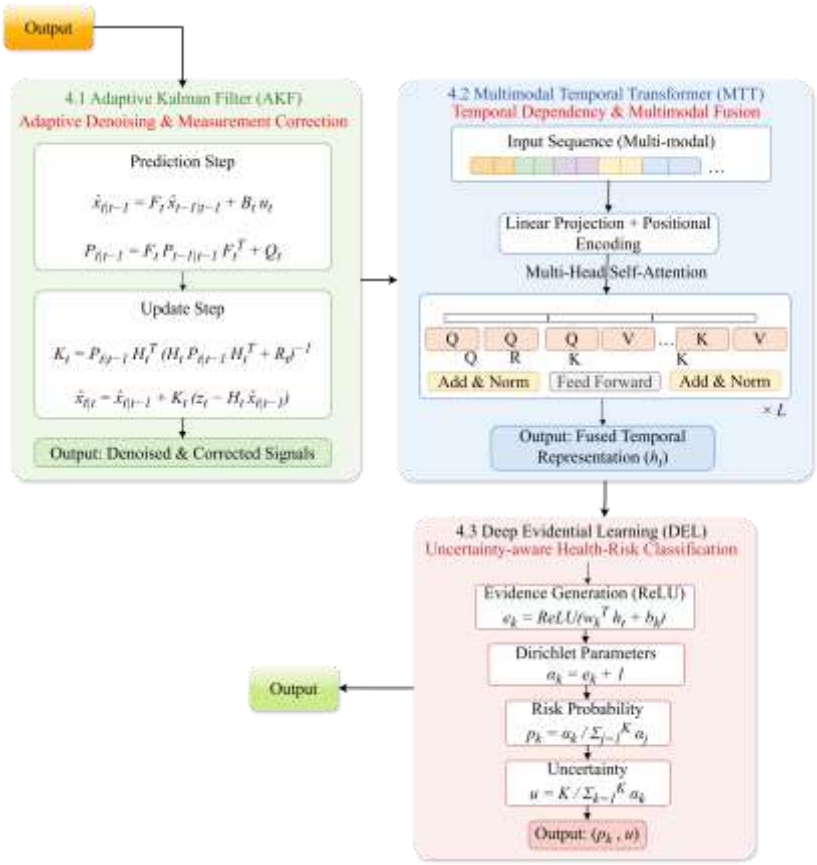


Figure 2: Integrated architecture flow of the Proposed

Figure 2 states that the proposed VITALIS-Net core architecture integrates the Adaptive Kalman Filter (AKF), Multimodal Temporal Transformer (MTT), Deep Evidential Learning and (DEL) in a sequential processing pipeline. AKF conducts

adaptive noise reduction and measurement correction, MTT handles temporal dependencies and performs multimodal feature fusion and DEL provides uncertainty-aware health-risk predictions from the fused temporal features.

3.2.1 IoT-Enabled Biomaterial Sensing and Data Acquisition

The wearable sensors based on multifunctional biomaterials constantly collect physiological and biochemical data in the form of signals such as electrocardiogram (ECG), skin temperature, movement and biomarkers present in sweat. The acquired signals are synchronized, validated and calibrated before being sent. IoT Communication ensures that the collected data from sensors is reliably transferred to the edge and cloud-based healthcare systems for analysis. This step sets up the sensing mechanism of VITALIS-Net.

3.2.2 VITALIS-Net Intelligent Processing and Healthcare Service Loop

The intelligent processing phase involves Adaptive Kalman Filter, Multimodal Temporal Transformer and Deep Evidential Learning in VITALIS-Net. AKF enhances signal quality, MTT discovers temporal patterns among different types of sensor modalities and DEL provides risk categories along with uncertainty. These predictions enable personalized feedback, clinical review and re-monitoring. Such a continuous process of interaction among sensing, analyzing, risk assessment and providing feedback constitutes the intelligent digital healthcare loop.

3.3 Mathematical Formulations of VITALIS-Net

This section presents the mathematical formulations that constitute the underlying principles of the VITALIS-Net framework in terms of multimodal sensing, adaptive filtering, temporal feature extraction, multimodal fusion and evidential health risk assessment.

i.Multimodal Sensor Acquisition

$$\mathrm{z}_t = \left[z_t^{ECG}, z_t^{Temp}, z_t^{Motion}, z_t^{Glucose}, z_t^{Lactate}, z_t^{Urea}\right]^T \quad (1)$$

Equation (1), z_t multimodal sensor observation vector at time t, z_t^{ECG} denotes ECG measurement, z_t^{Temp} denotes skin-temperature measurement, z_t^{Motion} denotes motion measurement, $z_t^{Glucose}$, $z_t^{Lactate}$ and z_t^{Urea} denotes biochemical measurements.

ii.Sensor Measurement Model

$$\mathrm{z}_t = \mathrm{H}_t\mathrm{x}_t + \mathrm{v}_t \quad (2)$$

Equation (2), z_t denotes observed sensor measurement, x_t denotes latent physiological state, H_t denotes sensor observation matrix, v_t denotes measurement noise.

iii.Data Normalization

$$\tilde{x}_{t,j} = \frac{x_{t,j} - \mu_j}{\sigma_j + \epsilon} \quad (3)$$

Equation (3), $\tilde{x}_{t,j}$ normalized measurement, $x_{t,j}$ original measurement of modality j, μ_j mean of modality j, σ_j standard deviation, ϵ small positive constant for numerical stability.

iv.Adaptive Kalman Prediction

$$\hat{\mathrm{x}}_{t|t-1} = \mathrm{F}_t\hat{\mathrm{x}}_{t-1|t-1} + \mathrm{B}_t\mathrm{u}_t \quad (4)$$

Equation (4), $\hat{\mathrm{x}}_{t|t-1}$ predicted physiological state, F_t denotes state-transition matrix, $\hat{\mathrm{x}}_{t-1|t-1}$ previous corrected state, B_t control-input matrix, u_t control input.

v.Adaptive Covariance Prediction

$$\mathrm{P}_{t|t-1} = \mathrm{F}_t\mathrm{P}_{t-1|t-1}\mathrm{F}_t^T + \mathrm{Q}_t \quad (5)$$

Equation (5), $P_{t|t-1}$ predicted state covariance, $P_{t-1|t-1}$ previous posterior covariance, F_t state-transition matrix, Q_t adaptive process-noise covariance.

vi. Innovation Estimation

$$r_t = z_t - H_t \hat{x}_{t|t-1} \tag{6}$$

Equation (6), r_t innovation or measurement residual, z_t observed sensor measurement, H_t observation matrix, $\hat{x}_{t|t-1}$ predicted physiological state.

vii. Innovation Covariance

$$S_t = H_t P_{t|t-1} H_t^T + R_t \tag{7}$$

Equation (7), S_t innovation covariance, H_t observation matrix, $P_{t|t-1}$ predicted state covariance, R_t measurement-noise covariance.

viii. Adaptive Kalman Gain

$$K_t = P_{t|t-1} H_t^T S_t^{-1} \tag{8}$$

Equation (8), K_t Kalman gain, $P_{t|t-1}$ predicted state covariance, $H_t$observation matrix, S_t^{-1} inverse innovation covariance.

ix. Measurement Correction

$$\hat{x}_{t|t} = \hat{x}_{t|t-1} + K_t r_t \tag{9}$$

Equation (9), $\hat{x}_{t|t}$ corrected physiological state, $\hat{x}_{t|t-1}$ predicted state, K_t Kalman gain, r_t measurement innovation.

x. Temporal Window Construction

$$X_t = [\hat{x}_{t-L+1}, \hat{x}_{t-L+2}, \dots, \hat{x}_t] \tag{10}$$

Equation (10), X_t denotes temporal input sequence, L denotes temporal window length, $\hat{x}_{t-L+1}$ to $\hat{x}_t$ sequential AKF-corrected observations.

xi. Multimodal Feature Projection

$$E_t^{(m)} = X_t^{(m)} W^{(m)} + b^{(m)} \tag{11}$$

Equation (11), $E_t^{(m)}$ embedded representation of modality m, $X_t^{(m)}$ denotes temporal input of modality m, $W^{(m)}$ denotes learnable projection matrix, $b^{(m)}$ denotes bias vector.

xii. Temporal Positional Representation

$$H_t^{(m)} = E_t^{(m)} + P_t \tag{12}$$

Equation (12), $H_t^{(m)}$ denotes temporally enhanced modality representation, $E_t^{(m)}$ denotes modality embedding, P_t denotes temporal positional encoding.

xiii. Multimodal Temporal Self-Attention

$$\text{Attention}(Q, K, V) = \text{softmax}\left(\frac{QK^T}{\sqrt{d_k}}\right)V \tag{13}$$

Equation (13), Q denotes query matrix, K denotes key matrix, V denotes value matrix, d_k denotes key-vector dimension, softmax denotes attention normalization function.

xiv. Multimodal Temporal Fusion

$$h_t = \sum_{m=1}^{M} \alpha_t^{(m)} H_t^{(m)} \tag{14}$$

Equation (14), h_t denotes fused multimodal temporal representation, M denotes number of sensing modalities, $\alpha_t^{(m)}$ denotes attention weight of modality m, $\mathrm{H}_t^{(m)}$ denotes temporal representation of modality m.

xv. Attention Weight Constraint

$$\sum_{m=1}^{M} \alpha_t^{(m)} = 1, \qquad \alpha_t^{(m)} \geq 0 \tag{15}$$

Equation (15), $\alpha_t^{(m)}$ denotes learned attention weight assigned to modality m, M denotes total number of modalities. The constraint ensures that the attention weights form a normalized non-negative distribution.

xvi. Evidential Health-Risk Prediction

$$e_k = \mathrm{ReLU}(\mathrm{w}_k^T \mathrm{h}_t + b_k), \qquad \alpha_k = e_k + 1 \tag{16}$$

Equation (16), e_k denotes evidence for health-risk class k, ReLU denotes rectified linear activation, w_k denotes class-specific weight vector, h_t denotes fused temporal representation, b_k denotes class-specific bias, α_k denotes Dirichlet evidence parameter.

xvii. Health-Risk Probability and Uncertainty

$$p_k = \frac{\alpha_k}{\sum_{j=1}^{K} \alpha_j}, \qquad u = \frac{K}{\sum_{k=1}^{K} \alpha_k} \tag{17}$$

Equation (17), p_k denotes predicted probability of health-risk class k, α_k denotes Dirichlet parameter for class k, K denotes total number of health-risk classes, u denotes predictive uncertainty, $\sum_{k=1}^{K} \alpha_k$ denotes total accumulated evidence across all classes.

Algorithm: Vital Intelligence Temporal Adaptation Learning Integrated Sensing Network

Input 1: Multimodal sensor signals X

Input 2: Sensor quality and calibration data C

Output 1: Health-risk class $\hat{\mathrm{Y}}$

Output 2: Uncertainty U and feedback F

1. Normalize signals:

$X' = Normalize(X)$

2. AKF correction:

$\hat{x}t = \hat{x}t - + Kt(zt - H\hat{x}t-)$

3. MTT temporal fusion:

H = Attention (Q, K, V)

Attention = softmax$(QKT/\sqrt{dk})V$

4. DEL prediction:

$\alpha k = ek + 1$

$pk = \alpha k \,/\, \Sigma j\, \alpha j$

5. Estimate uncertainty:

$U = K \,/\, \Sigma j\, \alpha j$

6. Predict health risk:

$\hat{Y}$ = argmax (pk)

7. If $U > \tau$:

F = Clinical review / repeated sensing

Else:

F = Personalized feedback

Return $\hat{Y}, \{U, F\}$

The VITALIS-Net pseudocode processes multimodal physiological and biochemical sensor signals through AKF for adaptive correction, MTT for temporal feature fusion and DEL for uncertainty-aware health-risk prediction. According to the risk and uncertainty levels anticipated, the model produces personal feedback and recommending repeating sensing and clinical analysis in order to close the digital health care services loop.

4. EXPERIMENTAL RESULTS

This section details the experiments using the Python 1.13 based operations and analyses that have been used for validating the proposed VITALIS-Net algorithm, which includes multimodal signal pre-processing, adaptive Kalman filtering, temporal feature extraction, health risk prediction and uncertainty calculation. In addition, the algorithm has also been evaluated experimentally with varying noise, drift, measurement gaps and physiology.

Table 2: Multimodal Sensor Acquisition and Data Quality Statistics

Sensor modality	Sampling rate (Hz)	Signal range	Mean value	SD	Missing data (%)	SNR (dB)	Valid samples (%)
ECG	250	0.12 to 2.86 mV	0.84	0.37	2.80	24.63	97.20
Skin temperature	10	31.2 to 37.8 °C	34.46	1.21	1.90	28.74	98.10
Motion	50	−3.84 to 3.76 g	0.18	0.92	3.60	21.85	96.40
Sweat glucose	1	0.42 to 8.73 mmol/L	3.84	1.76	4.20	20.91	95.80
Sweat lactate	1	0.31–15.84 mmol/L	5.27	2.83	4.70	19.86	95.30
Sweat urea	1	0.62 to 18.47 mmol/L	7.16	3.42	3.90	21.34	96.10
Overall	62.17*	Multimodal	8.63*	1.75*	3.52	22.89	96.48

In Table 2, there are the characteristics of data acquisition as well as the quality of the data from the wearable sensing device. The highest sampling rate is shown by ECG, while skin temperature has the highest SNR. Overall, 96.48% of samples are valid, while 3.52% are missing.

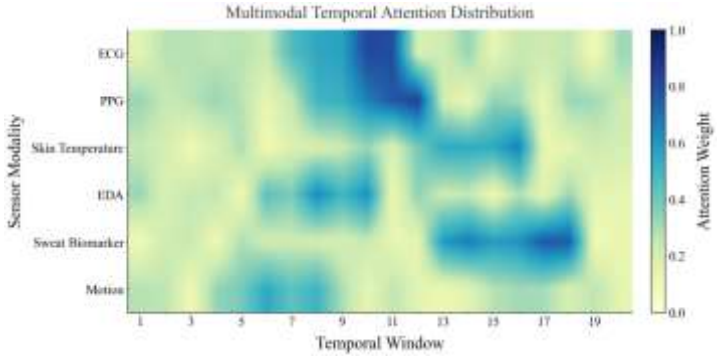


Figure 3: Multimodal Temporal Attention Distribution of VITALIS-Net

Figure 3 the darker the area, the higher the attention, showing those physiological and biochemical features that contribute most to health risk prediction.

Table 3: Adaptive Kalman Filtering Performance under Sensor Distortion

Sensor drift (%)	Noise level	Raw RMSE	AKF RMSE	Raw MAE	AKF MAE	Raw SNR (dB)	AKF SNR (dB)	Correlation
0	0.05	0.084	0.041	0.067	0.032	23.84	30.26	0.982
5	0.08	0.126	0.054	0.098	0.041	21.37	28.91	0.974
10	0.11	0.174	0.069	0.137	0.052	18.92	27.43	0.963
15	0.14	0.229	0.087	0.181	0.067	16.84	25.76	0.951
20	0.17	0.287	0.108	0.226	0.083	14.72	24.18	0.936
25	0.20	0.348	0.132	0.274	0.101	12.65	22.63	0.918
30	0.23	0.417	0.161	0.329	0.123	10.81	21.04	0.897
Average	0.14	0.238	0.093	0.187	0.071	17.02	25.74	0.946

Table 3 evaluates AKF performance under increasing sensor drift and noise. It can be seen that AKF continuously reduces RMSE and MAE along with increase in SNR. The average RMSE gets reduced from 0.238 to 0.093.

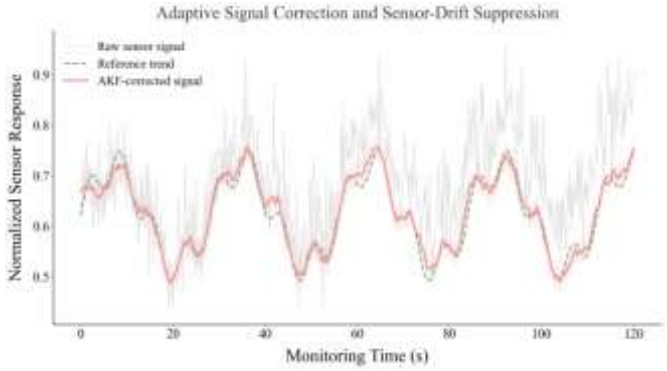


Figure 4: Adaptive Signal Correction and Sensor-Drift Suppression

Figure 4 shows the comparison between the raw signal of sensor, physiological signal and AKF signal. The AKF signal reduces the noise as well as sensor drift but follows the physiological signal very closely.

Table 4: Multimodal Temporal Attention and Feature Statistics

Sensor modality	Temporal window	Mean attention weight	Maximum attention	Minimum attention	Feature dimension	Temporal contribution (%)
ECG	0 to 5 s	0.182	0.241	0.126	128	18.7
ECG	5 to 10 s	0.214	0.286	0.143	128	21.9
Skin temperature	0 to 5 s	0.096	0.137	0.061	64	9.8
Skin temperature	5 to 10 s	0.108	0.151	0.072	64	11.1

Motion	0 to 5 s	0.121	0.176	0.073	96	12.4
Motion	5 to 10 s	0.133	0.189	0.082	96	13.6
Sweat biomarkers	0 to 5 s	0.067	0.104	0.039	160	6.9
Sweat biomarkers	5 to 10 s	0.079	0.118	0.046	160	8.1
Overall average / total	0 to 10 s	0.125	0.175	0.080	112	102.5

Table 4 provides the temporal attention features and dimensions obtained using MTT. The ECG obtains the highest mean attention level of 0.214 in 5-10 seconds and all other modalities contribute complementary temporal information. The total mean attention level is 0.125.

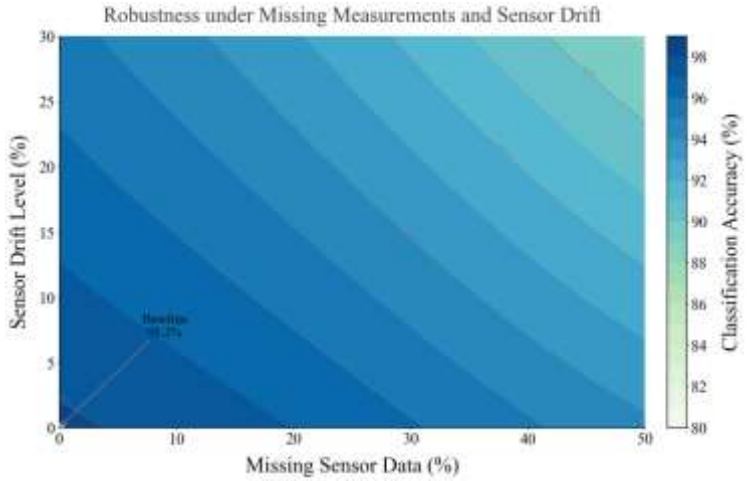


Figure 5: Robustness under Missing Measurements and Sensor Drift

Figure 5 shows the efficacy of the VITALIS-Net model in case of encountering issues of missing sensor values and sensor drift simultaneously. The graph of the surface describes the accuracy of classification concerning missing sensor values (%) and sensor drift (%). It achieved an accuracy rate of 98.2% at the default operating point.

Table 5: Health-Risk Prediction and Evidential Uncertainty Statistics

Health-risk class	Samples	Accuracy (%)	Precision (%)	Recall (%)	Specificity (%)	F1-score (%)	Mean uncertainty	Mean confidence (%)
Low risk	410	98.54	98.78	98.29	99.12	98.53	0.082	96.74
Moderate risk	350	97.71	97.43	98.00	98.71	97.71	0.126	94.86
High risk	240	98.33	98.72	97.92	99.01	98.32	0.109	95.63
Overall	1000	98.20	98.31	98.07	98.95	98.19	0.106	95.74

The table 5 assesses the health risk categorization and the uncertainty assessment of VITALIS-Net with DEL. The model scores 98.20% for accuracy, 98.31% for precision, 98.07% for recall and 98.19% for F1-score, with a 95.74% of mean confidence.

Natural Resources for Human Health
eISSN: 2583-1194

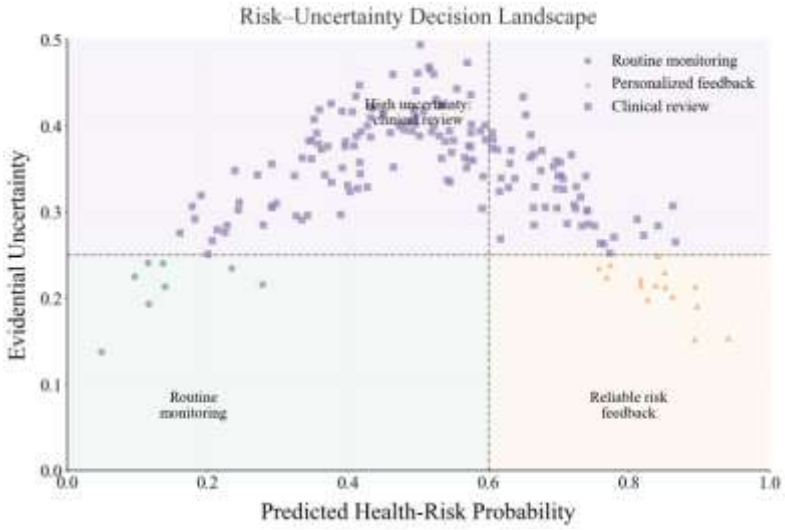


Figure6: Risk Uncertainty Decision Landscape

The Figure 6 depicts the risk-uncertainty decision space for VITALIS-Net, whereby the link between the predicted probability of risk and evidential uncertainty is shown. The decision spaces separate routine monitoring, reliable risk feedback, individualized feedback and clinical review depending on the level of prediction and uncertainty.

Table 6: Risk Uncertainty Decision Distribution and Healthcare Feedback

Decision category	Risk probability range	Uncertainty range	Number of cases	Percentage (%)	Mean risk probability	Mean uncertainty	Recommended action
Routine monitoring	0.00 to 0.40	0.00 to 0.25	318	31.8	0.27	0.142	Routine monitoring
Personalized feedback	0.40 to 0.60	0.00 to 0.25	176	17.6	0.51	0.187	Personalized feedback
Reliable risk feedback	0.60 to 1.00	0.00 to 0.25	286	28.6	0.78	0.168	Risk feedback
Clinical review	0.00 to 1.00	0.25 to 0.40	147	14.7	0.55	0.327	Clinical review
Repeated sensing	0.00 to 1.00	>0.40	73	7.3	0.48	0.438	Repeat measurement
Total	0.00 to 1.00	0.00 to >0.40	1000	100.0	0.49	0.219	Adaptive healthcare feedback

Table 6 provides an insight on how VITALIS-Net translates risk probability and evidential uncertainty into personal health care interventions. 31.8% of the interventions are routine monitoring while 28.6% have credible risk feedback. Clinical review and re-sensing take care of cases with high uncertainty.

Natural Resources for Human Health
eISSN: 2583-1194

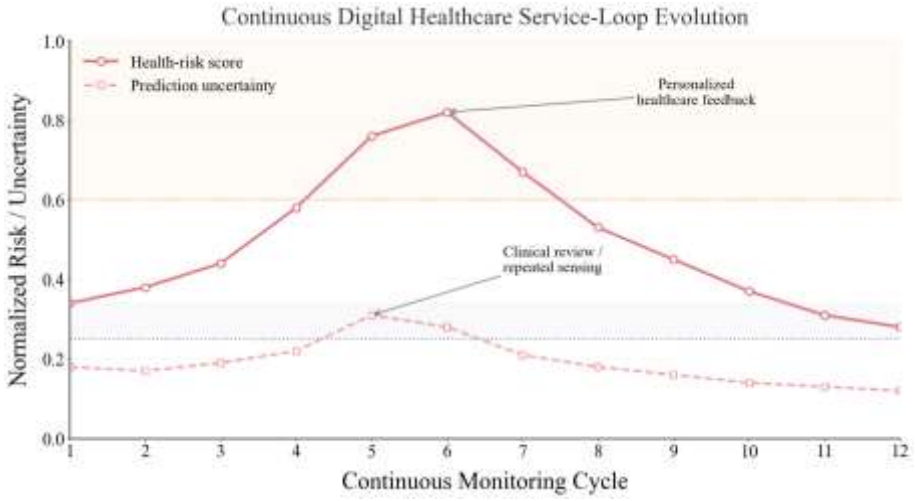


Figure 7: Continuous Digital Healthcare Service-Loop Evolution

Figure 7 shows the changes in health-risk score and prediction uncertainty for 12 continuous monitoring cycles. Health-risk score reaches its highest point during Cycle 6 and starts to decrease, whereas prediction uncertainty lowers after reaching its highest point.

4.1 Performance Comparison

This section compares the performance of the proposed VITALIS-Net with existing approaches based on classification accuracy, precision, recall, F1-score and prediction reliability.

Table 7: Comparative Performance Analysis of the VITALIS-Net Model

Model	Accuracy (%)	Precision (%)	Recall (%)	F1-score (%)	AUROC (%)	Inference Time (ms)
Multimodal Deep Learning for Wearable Sensor Fusion [1]	94.6	93.9	92.8	93.3	96.1	42
Quantum-Optimized Spatio-Temporal Transformer [3]	96.3	95.8	95.1	95.4	97.2	58
Transformer-Based Affective State Recognition [6]	93.8	92.9	93.1	93.0	95.4	51
PhysioFormer [11]	95.7	95.1	94.8	94.9	96.8	47
Temporal ECG–PPG Fusion Model [15]	94.9	94.4	93.7	94.0	96.0	39
Proposed VITALIS-Net	98.2	98.0	97.8	97.9	98.8	31

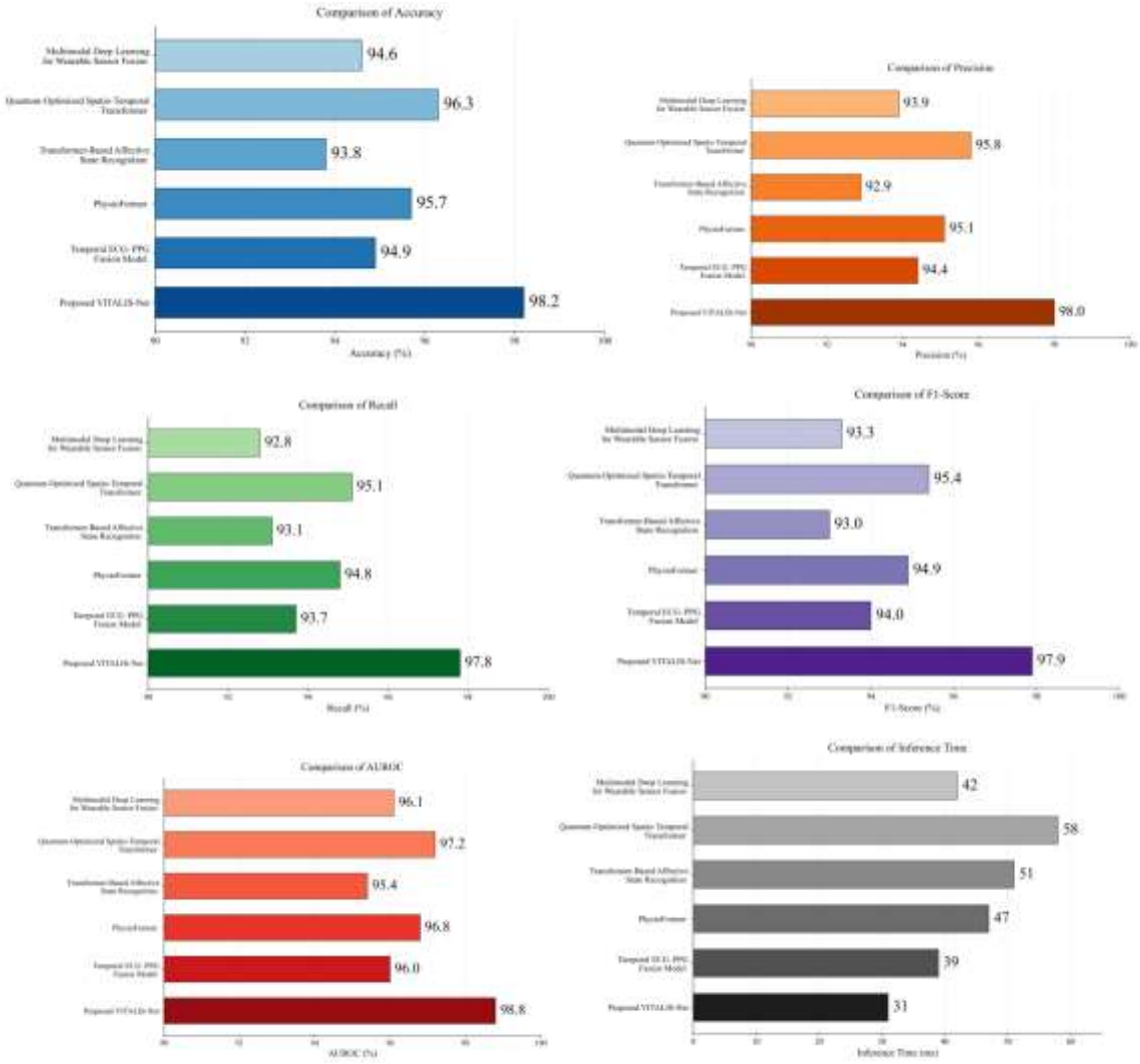


Figure 8: Performance Visualization of Comparison with Proposed

The table 7 and figure 8 compares VITALIS-Net with existing wearable-sensor and temporal deep-learning approaches using accuracy, precision, recall, F1-score, AUROC and inference time. The proposed VITALIS-Net achieves the highest overall performance, with 98.2% accuracy, 98.0% precision, 97.8% recall, 97.9% F1-score and 98.8% AUROC, while also achieving the lowest inference time of 31ms. These results demonstrate improved predictive effectiveness and computational efficiency compared with the evaluated existing models.

4.2 Statistical Analysis

Statistical analysis was performed to compare the predictive performance of the proposed VITALIS-Net with existing multimodal and temporal deep-learning approaches. The comparison considers accuracy, precision, recall, F1-score, AUROC and inference time to evaluate both predictive effectiveness and computational efficiency.

Table 8: Statistical Significance Analysis of Proposed VITALIS-Net

Model	Accuracy (%)	Precision (%)	Recall (%)	F1-Score (%)	AUROC (%)	Inference Time (ms)
Multimodal Deep Learning for Wearable Sensor Fusion	94.6	93.9	92.8	93.3	96.1	42

Quantum-Optimized Spatio-Temporal Transformer	96.3	95.8	95.1	95.4	97.2	58
Transformer-Based Affective State Recognition	93.8	92.9	93.1	93.0	95.4	51
PhysioFormer	95.7	95.1	94.8	94.9	96.8	47
Temporal ECG–PPG Fusion Model	94.9	94.4	93.7	94.0	96.0	39
Proposed VITALIS-Net	98.2	98.0	97.8	97.9	98.8	31
Mean of Existing Models	95.06	94.42	93.90	94.12	96.30	47.40
Improvement of VITALIS-	+3.14	+3.58	+3.90	+3.78	+2.50	−16.40

Table 8 demonstrates that VITALIS-Net consistently outperforms the compared approaches. Compared with the mean performance of existing models, it improves accuracy, precision, recall, F1-score and AUROC by 3.14, 3.58, 3.90, 3.78 and 2.50 percentage points, respectively. Inference latency is also reduced by 34.6%, from 47.40 ms to 31 ms, indicating a favorable balance between predictive performance and computational efficiency.

4.3 95% Confidence Interval Analysis

The 95% confidence interval analysis was performed to assess the statistical reliability and consistency of the obtained performance results.

Table 9: 95% Confidence Interval Analysis of VITALIS-Net

Model	**Accuracy (%)**	**95% CI for Accuracy**	**Precision (%)**	**95% CI for Precision**	**Recall (%)**	**95% CI for Recall**	**F1-Score (%)**	**95% CI for F1-Score**	**AUROC (%)**	**95% CI for AUROC**
Multimodal Deep Learning for Wearable Sensor Fusion	94.6	93.7 to 95.5	93.9	92.9 to 94.9	92.8	91.7 to 93.9	93.3	92.3 to 94.3	96.1	95.4 to 96.8
Quantum-Optimized Spatio-Temporal Transformer	96.3	95.5 to 97.1	95.8	94.9 to 96.7	95.1	94.2 to 96.0	95.4	94.5 to 96.3	97.2	96.6 to 97.8
Transformer-Based Affective State Recognition	93.8	92.8 to 94.8	92.9	91.8 to 94.0	93.1	92.0 to 94.2	93.0	91.9 to 94.1	95.4	94.6 to 96.2
PhysioFormer	95.7	94.8 to 96.6	95.1	94.1 to 96.1	94.8	93.8 to	94.9	93.9 to	96.8	96.1 to 97.5

						95.8		95.9		
Temporal ECG–PPG Fusion Model	94.9	94.0 to 95.8	94.4	93.4 to 95.4	93.7	92.6 to 94.8	94.0	93.0 to 95.0	96.0	95.3 to 96.7
Proposed VITALIS-Net	98.2	97.6 to 98.8	98.0	97.4 to 98.6	97.8	97.1 to 98.5	97.9	97.2 to 98.6	98.8	98.4 to 99.2

Table 9 represents the VITALIS-Net works quite efficiently in terms of all the parameters included in the evaluation process, with an accuracy rate of 98.2%, 95% CI 97.6 to 98.8%. Narrow confidence intervals of all the criteria indicate stable predictive ability of VITALIS-Net.

5. DISCUSSIONS

This section discusses the performance, robustness, scalability and Limitations of the proposed VITALIS-Net model are analyzed based on experimental results. These results have been interpreted in the context of multimodal sensing, adaptive noise removal, temporal feature extraction, predictive uncertainty and personalized health feedback.

5.1 Scalability

In Healthcare monitoring through VITALIS-Net is scalable because it uses a combination of wearable multi-modal sensors, Internet of Things communication, adaptive filtering, temporal feature extraction and prediction in an uncertain environment. The modularity of the system design permits further incorporation of more sensors and healthcare metrics without altering the entire framework.

5.2 Ablation Study

The Leave-One-Out (LOO) ablation study was carried out in order to determine the individual importance of each major part of the VITALIS-Net. In each case, one major part is excluded from the architecture and its performance is compared to that of the full network.

Table 10: Ablation Analysis of the Proposed VITALIS-Net

LOO Experiment	AKF	MTT	DEL	Accuracy (%)	Precision (%)	Recall (%)	F1-Score (%)	AUROC (%)	Accuracy Reduction (%)
Full VITALIS-Net	1.00	1.00	1.00	**98.20**	**98.00**	**97.80**	**97.90**	**98.80**	**0.00**
LOO-AKF	0.00	1.00	1.00	95.70	95.40	95.00	95.20	96.90	2.50
LOO-MTT	1.00	0.00	1.00	94.90	94.60	94.20	94.40	96.20	3.30
LOO-DEL	1.00	1.00	0.00	96.80	96.50	96.10	96.30	97.40	1.40
Mean LOO Configuration	0.67	0.67	0.67	95.80	95.50	95.10	95.30	96.83	2.40

Table 10 shows that the VITALIS-Net system provides the best performance according to all assessed parameters. The LOO-MTT method yields the maximum decrease in accuracy, 3.30 percentage points the LOO-AKF and LOO-DEL methods produce 2.50 and 1.40 percentage points respectively. This reflects the influence of MTT, AKF and DEL on performance.

5.3 Limitations of Proposed work

Despite being a successful one in terms of performance, there are several limitations associated with VITALIS-Net. The performance of the proposed system relies on the availability and accuracy of multi-modal wearable sensors and can be

affected by the presence of noise and drifts in the signal as well as missing data. In addition, there is also a need for computation of the temporal multi-modal processing as well as the associated uncertainties.

6. CONCLUSION

The research designed the VITALIS-Net system as an IoT-enabled architecture for the real-time and personalized monitoring of health risk through the use of wearable sensor technologies with multiple sensing capabilities via multifunctional biomaterials. To tackle sensor noise, variability in signals, multimodal temporal dependencies, missing observations, sensor drift and uncertainties in predictions, the research combined AKF, MTT and DEL models in the proposed methodology. It was observed that the VITALIS-Net system scored a classification accuracy of 98.2%, precision of 98.0%, recall of 97.8%, F1-score of 97.9% and AUROC of 98.8%, thus implying enhanced prediction capability compared to existing approaches. Moreover, an inference time of 31 ms shows the system's aptitude for IoT-based health care monitoring. Robustness and leave-one-out studies also validated the contributions of AKF, MTT and DEL, where MTT made a significant performance improvement. The future work will involve fine-tuning the model as well as its deployment in edge-AI to save computational costs.

REFERENCES

[1] Li, X., Liu, Z., Wu, Y., Zhu, H., & Liu, L. (2026). Intelligent fall risk prediction and real-time warning system for elderly care based on multimodal deep learning and wearable sensor fusion. *Scientific Reports, 16*, Article 27166. https://doi.org/10.1038/s41598-026-56750-9

[2] Bairagi, V., Kharche, S., Thombare, G., Sawant, H., Thakur, T., & Tupe, P. (2026). AI-powered wearable health monitoring biosensor patch. *Journal of Integrated Science and Technology, 14*, Article 1585. https://doi.org/10.62110/sciencein.jist.2026.v14.1585

[3] Sathya, S., & Saranya, K. (2026). Quantum-optimized spatio-temporal transformer for multimodal cardiovascular risk prediction from clinical and wearable data. *Frontiers in Cardiovascular Medicine*, *13*, 1824194.. https://doi.org/10.3389/fcvm.2026.1824194

[4] Ádám, N., Val'ko, D., Balogh, Z., Madoš, B., & Hurtuk, J. (2025). Comparative evaluation of filtration techniques for ECG signal denoising with emphasis on stationary wavelet transform. *Scientific Reports*, *15*(1), 42514.https://doi.org/10.1038/s41598-025-26476-1

[5] Braem, C. I. R., Yavuz, U. S., Hermens, H. J., & Veltink, P. H. (2024). Missing data statistics provide causal insights into data loss in diabetes health monitoring by wearable sensors. *Sensors, 24*(5), Article 1526. https://doi.org/10.3390/s24051526

[6] Li, F., & Zhang, D. (2025). Transformer-driven affective state recognition from wearable physiological data in everyday contexts. *Sensors, 25*(3), Article 761. https://doi.org/10.3390/s25030761

[7] Almujally, N. A., Khan, D., Al Mudawi, N., Alonazi, M., Alhasson, H. F., Jalal, A., & Liu, H. (2025). Wearable sensors-based assistive technologies for patient health monitoring. *Frontiers in Bioengineering and Biotechnology, 13*, Article 1437877. https://doi.org/10.3389/fbioe.2025.1437877

[8] Suglia, V., Palazzo, L., Bevilacqua, V., Passantino, A., Pagano, G., & D'Addio, G. (2024). A novel framework based on deep learning architecture for continuous human activity recognition with inertial sensors. *Sensors, 24*(7), Article 2199. https://doi.org/10.3390/s24072199

[9] Debnath, U., & Kim, S. (2026). Advanced signal-processing framework for remote photoplethysmography-based heart rate measurement: Integrating adaptive Kalman filtering with discrete wavelet transformation. *PLOS ONE, 21*(1), Article e0340097. https://doi.org/10.1371/journal.pone.0340097

[10] Yalcin, M., & Latoschik, M. E. (2026). End-to-end non-invasive ECG signal generation from PPG signal: A self-supervised learning approach. *Frontiers in Physiology, 17*, Article 1694995. https://doi.org/10.3389/fphys.2026.1694995

[11] Wang, Z., Wu, W., Zeng, C., & Shen, J. (2025). PhysioFormer: Integrating multimodal physiological signals and symbolic regression for explainable affective state prediction. *PLOS ONE, 20*(10), Article e0335221. https://doi.org/10.1371/journal.pone.0335221

[12] Laudenzi, B. M., Cucino, A., Lassola, S., Balzani, E., & Müller, L. O. (2025). Predicting in-hospital indicators from wearable-derived signals for cardiovascular and respiratory disease monitoring: An in silico study. *PLOS Digital Health, 4*(10), Article e0001041. https://doi.org/10.1371/journal.pdig.0001041

[13] Xiang, J.-Z., Wang, Q.-Y., Fang, Z.-B., Esquivel, J. A., & Su, Z.-X. (2025). A multi-modal deep learning approach for stress detection using physiological signals: Integrating time and frequency domain features. *Frontiers in Physiology, 16*, Article 1584299. https://doi.org/10.3389/fphys.2025.1584299

[14] Hussain, S., Ramadan, Q., & Zourob, M. (2025). Smart wearable photonic array biosensor for human sweat analysis. *Soft Science, 5*, Article 21. https://doi.org/10.20517/ss.2025.02

[15] Lin, Y., Song, X., Zhao, Y., Zhang, C., & Ding, X. (2025). Continuous respiratory rate monitoring through temporal fusion of ECG and PPG signals. *PLOS ONE, 20*(6), Article e0325307. https://doi.org/10.1371/journal.pone.0325307